J. Biochem. 2012;151(1):99–108 doi:10.1093/jb/mvr119

JB THE JOURNAL OF BIOCHEMISTRY

Microtubule-associated protein 4 binds to actin filaments and modulates their properties

Received April 4, 2011; accepted September 5, 2011; published online September 21, 2011

Kazuyuki Matsushima[1,*†], Kiyotaka Tokuraku[2,‡], Mohammad Rubayet Hasan[3,§] and Susumu Kotani[1]

[1]Department of Biological Sciences, Faculty of Science, Kanagawa University, Tsuchiya 2946, Hiratsuka, Kanagawa 259-1293; [2]Department of Chemical Science and Engineering, Miyakonojo National College of Technology, Yoshio-cho 473-1, Miyakonojo, Miyazaki 885-8567; and [3]Department of Bioscience and Bioinformatics, Faculty of Computer Science and Systems Engineering, Kyushu Institute of Technology, Kawazu 680-4, Iizuka, Fukuoka, 820-8502, Japan

*Kazuyuki Matsushima, Central Institute of Saravio Cosmetics Ltd., Tsurumi 1356-6, Beppu, Ooita 874-0840, Japan

†Kazuyuki Matsushima, Central Institute of Saravio Cosmetics Ltd, Tsurumi 1356-6, Beppu, Ooita 874-0840, Japan. Tel: +81-977-75-8575, email: kazuyuki_matsushima@yahoo.co.jp

‡Kiyotaka Tokuraku, Division of Applied Science and Engineering, Course of Biosystem, Graduate School of Muroran Institute of Technology, Mizumoto-cho 27-1, Muroran, Hokkaido 050-8585, Japan

§Mohammad Rubayet Hasan, Department of Medicine, University of British Columbia, 2775 Laurel Street, Vancouver, BC V5Z 1M9, Canada.

We previously reported that an isoform of microtubule-associated protein 4 (MAP4) is localized to the distal area of developing neurites, where microtubules are relatively scarce, raising the possibility that MAP4 interacts with another major cytoskeletal component, actin filaments. In the present study, we examined the *in vitro* interaction between MAP4 and actin filaments, using bacterially expressed MAP4 and its truncated fragments. Sedimentation assays revealed that MAP4 and its microtubule-binding domain fragments bind to actin filaments under physiological conditions. The apparent dissociation constant and the binding stoichiometry of the fragments to actin were about 0.1 μM and 1 : 3 (MAP4/actin), respectively. Molecular dissection studies revealed that the actin-binding site on MAP4 is situated at the C-terminal part of the proline-rich region, where the microtubule-binding site is also located. Electron microscopy revealed that the MAP4-bound actin filaments become straighter and longer and that the number of actin bundles increases with greater concentrations of added MAP4 fragment, indicating that MAP4 binding alters the properties of the actin filaments. A multiple sequence alignment of the proline-rich regions of MAP4 and tau revealed two putative actin-binding consensus sequences.

Keywords: actin-binding protein/MAPs/MAP4/microtubule-associated protein/proline-rich.

Abbreviations: CBB, Coomassie Brilliant Blue; EDC, 1-ethyl-3-(dimethylamino-propyl)-carbodiimide; MAP(s), microtubule-associated protein(s); MEM, a buffer consisting of 100 mM 2-(*N*-morpholino) ethanesulfonic acid (pH 6.8), 0.5 mM $MgSO_4$, 0.1 mM EGTA and 0.1 mM ATP; PBS, phosphate-buffered saline; Pro-rich, proline rich; PVDF, polyvinylidene fluoride; SDS–PAGE, SDS–polyacrylamide gel electrophoresis.

Microtubule-associated protein 4 (MAP4) is a major non-neural MAP that plays important roles in the intracellular organization of microtubules (*1*). MAP4 molecules appear as several alternatively spliced variants with differences in the microtubule-binding domain organizations (*2–4*). In 2005, we identified a new isoform with a defective proline-rich (Pro-rich) region (MAP4-SP), specific to neural-ectoderm-derived tissues (*4*). MAP4-SP exchanged rapidly between the microtubule-bound and unbound states, at a rate 2–4 times faster ($t_{1/2}$ ~5–9 s) than that of the conventional isoform (MAP4-LP) ($t_{1/2}$ ~16–22 s) (*5*). In addition, fluorescence microscopy showed that MAP4-SP expressed in neuroblastoma cells was often found in the distal area of developing neurites, where microtubules are relatively scarce (*6*). In primary cultures of cortical neurons, a patchy staining pattern of endogenous MAP4 is observed in the neural processes (*7*). These findings suggested that MAP4-SP contributes to the dynamics of developing neurites, by enhancing microtubule turnover and possibly by regulating the interactions between microtubules and other cytoskeletal components.

Cooperation between microtubules and actin filaments is important for diverse cellular events, including neurite outgrowth (*8*, *9*). When growth cones advance, retract or turn, the two major cytoskeletal systems are reorganized by numerous regulatory factors, with MAPs being the most probable candidates. Several MAPs reportedly interact with actin filaments. For instance, the light chains of MAP1A and MAP1B, major members of the MAP1 family, have an actin-binding region as well as microtubule-binding regions (*10*). MAP2 and tau also bind to actin filaments by their microtubule-binding domains (*11–14*). In contrast, the association of MAP4 with actin filaments *in vitro* has not been investigated since early attempts to detect their interaction were unsuccessful (*15*, *16*). Recently, actin aggresomes, generated by an actin-stabilizing toxin, were reported to be associated with microtubules, MAP4, and vimentin intermediate

Downloaded from http://jb.oxfordjournals.org/ at Changhua Christian Hospital on September 26, 2012

© The Authors 2011. Published by Oxford University Press on behalf of the Japanese Biochemical Society. All rights reserved

filaments *in vivo* (*17*), but direct evidence for the MAP4-actin interaction is still lacking.

In this study, we tested the actin-binding activity of MAP4. In contrast to previous results (*15*, *16*), our *in vitro* sedimentation assays indicated the direct interaction of MAP4 with actin filaments. Furthermore, we identified the region of MAP4 responsible for actin binding. The morphologies of the MAP4-bound actin filaments were also examined.

Materials and Methods

Materials

Oligonucleotides were purchased from Hokkaido System Science (Sapporo, Japan). Phosphate-buffered saline (PBS) was purchased from Gibco (Carlsbad, CA). All chemicals were of reagent grade, unless otherwise described.

Construction of expression plasmids

To construct the expression plasmid for the P_N fragment (containing residues 579–717 of bovine MAP4-LP), the plasmid containing the MAP4 cDNA (GenBank: AB354119) was cleaved with *Nco*I. The *Nco*I/*Nco*I end cDNA fragment was purified and ligated in-frame into the expression plasmid vector pET21d(+) (Stratagene, La Jolla, CA), which had been treated with the same enzyme. The expression plasmids for the Pj, LP and A_5T fragments (containing residues 1–578, 579–880 and 881–1098, respectively) were generated using the plasmid containing the full-length MAP4-LP as the template. The construction of the expression plasmid for the PcA_3 fragment, which was originally prepared for another study, will be described elsewhere (manuscript in preparation). Sequences were confirmed by complete sequencing of both DNA strands of each plasmid.

Protein preparation

The purification procedures for the full-length MAP4 and the truncated fragments were described previously (*3–6*). The LP, P, P_N, A_5T and P_CA_3 fragments were expressed in *E. coli* BL-21(DE3)pLysS (Stratagene, La Jolla, CA), transformed with the recombinant plasmids encoding the LP, P, P_N, A_5T and P_CA_3 fragments, respectively, and were purified by successive column chromatography steps on a phospho-cellulose (P-11,Whatman, Clifton, NJ) column and a hydrophobic column (TOYOPEARL Butyl-650 C, Tosoh, Japan), except for the Pj fragment, which was purified by diethylaminoethyl-cellulose (DE-52, Whatman, Clifton, NJ) column chromatography. All recombinant MAP4 proteins were dialyzed against a buffer containing 100 mM 2-(*N*-morpholino) ethanesulfonic acid (pH 6.8), 0.5 mM $MgSO_4$, 0.1 mM EGTA, and 0.1 mM ATP (MEM buffer) and stored in liquid N_2. Rabbit skeletal muscle actin was prepared by the method of Spudich and Watt (*18*), stored in liquid N_2 and clarified by ultra-centrifugation at 100,000*g* for 1 h at 4°C before use. Protein concentrations were determined by the method of Lowry *et al*. (*19*), using BSA as the standard.

Protein detection

SDS–polyacrylamide gel electrophoresis (SDS–PAGE) was performed using 7.5, 10, 12.5 or 14% acrylamide gels, according to Laemmli (*20*). Gels were stained with Coomassie brilliant blue (CBB) R250. For the immunological analysis, samples on polyacrylamide gels were transferred to a polyvinylidene fluoride (PVDF) membrane (Immobilon-P, Millipore, Billerica, MA). The membrane was then probed with either anti-MAP4 antiserum (*21*) or an anti-actin antibody (A5060, Sigma-Aldrich, St. Louis, MO).

Sedimentation analysis

Actin was polymerized in advance in MEM buffer at 25°C, mixed with recombinant proteins, and incubated for 1 h at 25°C. The mixtures were centrifuged at 5,000*g* (low speed) for 30 min at 25°C to precipitate the actin bundles (Pellet of bundles, P_B), according to Meyer and Aebi (*22*). The supernatant thus obtained was then centrifuged at 100,000*g* (high speed) for 30 min at 25°C, to sediment the unbundled actin filaments (Pellet of filaments, P_F). The volumes of the P_B, P_F and final supernatant (S) fractions were equalized by supplementation with SDS sample buffer and were electrophoresed. Isoelectric focusing was performed with an immobilized pH 3–10 gradient strip in an electrophoretic apparatus (Model BE-410, Bio-Craft, Japan), according to the manufacturer's instructions. The strip was then loaded on the polyacrylamide gel for two-dimensional gel electrophoresis.

Chemical crosslinking of actin and the LPA_5T fragment

Purified actin (20 μM) and the LPA_5T fragment (2 μM) were mixed in MEM buffer supplemented with 1-ethyl-3-(dimethylamino-propyl)-carbodiimide (EDC, 5 mM), and the mixture was incubated for 1 h at 25°C. To inhibit actin polymerization, 40 μM of cytochalasin D (C8273, Sigma-Aldrich, St. Louis, MO) was added to the mixture. Aliquots were quenched with ammonium acetate (100 mM) and analysed by SDS–PAGE and immunoblotting.

Quantitative analyses

Various concentrations of MAP4 fragments and 10 μM actin were mixed in MEM buffer, and were incubated for 1 h at 25°C. The polymerized actin was collected by ultra-centrifugation at 100,000*g* for 30 min at 25°C, and the precipitate was resuspended in the original volume of MEM buffer. The following analysis was performed according to Tokuraku *et al*. (*23*).

Electron microscopy

Mixtures of actin and recombinant proteins were incubated for 30 min at 25°C. A 6 μl aliquot of the sample solution was adsorbed to a carbon-coated grid (Okenshoji Co. Ltd., Japan), stained with two drops of freshly prepared 1% uranyl acetate and observed under a JEOL JEM-2000EX electron microscope. Anti-MAP4 antiserum (*21*) and 10-nm gold-coupled goat anti-rabbit IgG (BB International, Cardiff, UK) were used for the immunogold labelling of MAP4.

The number of actin ends in 40 randomly chosen frames (0.5×0.5 μm) was counted, and the average number per 1 μm^2 and the standard error were calculated. More than 50 actin filaments were chosen at random from electron micrographs of three independent experiments, and the length of each actin filament was classified as either longer or shorter than 1 μm. To examine the linearity of the actin filaments, we randomly chose >100 filament segments longer than 500 nm and determined whether each filament could fit into a set frame (25 nm × 300 nm).

Multiple sequence alignment of the Pro-rich domains

The alignment of the bovine, human and murine MAP4 (GenBank: DAA16874.1, NCBI reference sequences: NP_002366.2 and NP_032659.2, respectively) and tau (NCBI reference sequences: NP_776531.1, NP_058525.1 and NP_001033698.1, respectively) sequences was constructed using the dynamic DNASIS™ Pro program, version 2.07 (Hitachi Software Engineering, Japan) and was manually refined.

Results

Preparation of the MAP4 isoforms and their fragments

The primary structures of the two full-length MAP4 isoforms and the truncated fragments used in this study are illustrated in Fig. 1A. Along with the MAP4 fragments described elsewhere [the LPA_5T, LPA_4T, LPA_3T (*3*), SPA_5T (*4*), P (*23*) and PcA_3 fragments], we newly generated expression plasmids for the Pj, LP, A_5T and P_N fragments. These proteins were purified to homogeneity (Fig. 1B), except for MAP4-LP, MAP4-SP and the Pj fragment (Fig. 1B, lanes 1, 2 and 4). Several lower molecular mass bands, which all reacted with anti-MAP4 antiserum (*21*) (Fig. 1B, lanes 5, 6 and 8), could not be removed from these three samples. However, since no bands with a molecular mass >75 kDa were detected in a heat-stable fraction of the untransfected bacterial extract (Fig. 1B, lane 3), these contaminating proteins were presumably the proteolytic products of the full-length recombinant proteins. Since bovine MAP4 was identified as the

Downloaded from http://jb.oxfordjournals.org/ at Changhua Christian Hospital on September 26, 2012

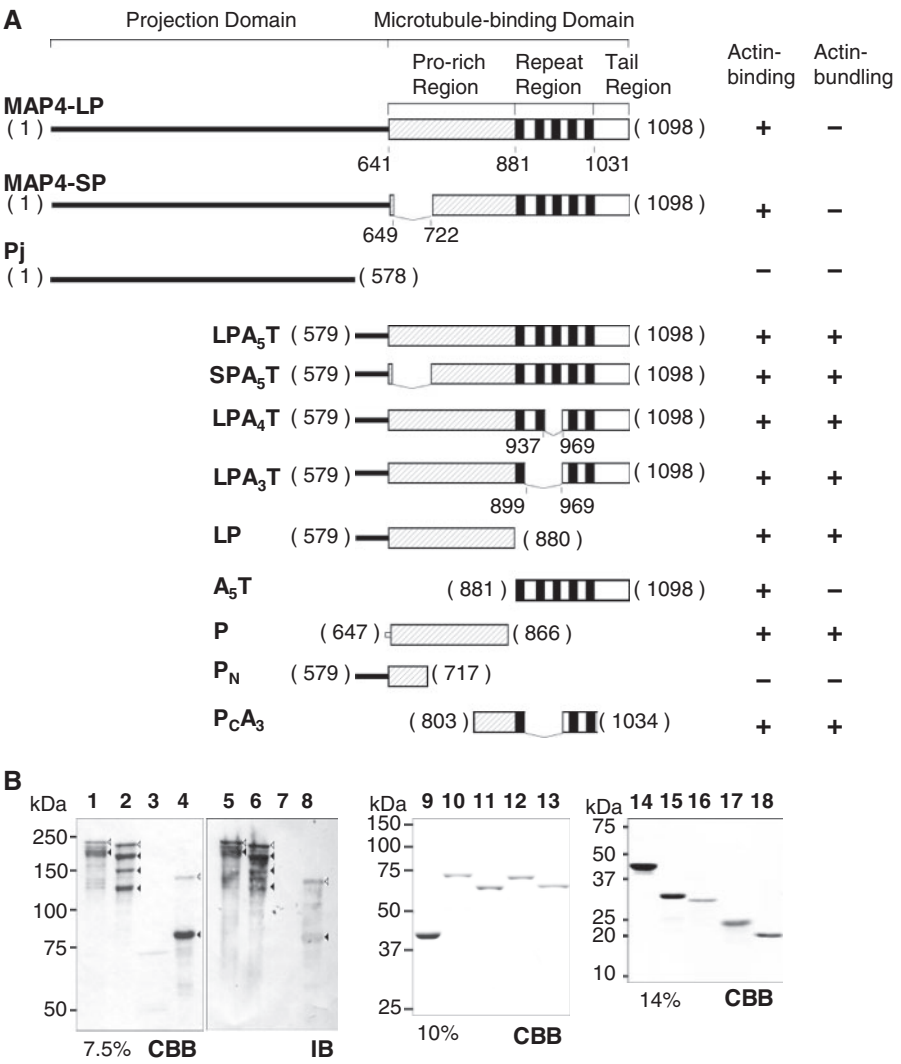

Fig. 1 Schematic structures and representative SDS-PAGE patterns of the proteins used in this study. (A) Schematic structures of the full-length bovine MAP4 isoforms (MAP4-LP and MAP4-SP) and the truncated fragments (Pj, LPA_5T, SPA_5T, LPA_4T, LPA_3T, LP, A_5T, P, P_N and P_CA_3). Arabic numerals in the figures are the amino acid residue numbers. The N- and C-terminal amino acid residue numbers are indicated by the numbers in parentheses on both sides of each fragment. The short N-terminal region of the P fragment, drawn as a thin, open box, is an additional sequence derived from the lac'Z gene and the polylinker site of pUC. The nomenclatures of the fragments and the subdomains are according to our previous reports (*3*, *4*, *23*). The actin-bundling and actin-binding activities of the proteins are shown on the right side of the figures as plus or minus signs. (B) Electrophoretic patterns of the purified proteins. The proteins in lanes 1–4 and 9–18 are visualized by CBB staining, while those in lanes 5–8 are immunoblotted by anti-MAP4 antiserum (*21*). Lanes 1 and 5, MAP4-LP; lanes 2 and 6, MAP4-SP; lanes 3 and 7, heat-stable fraction of untransformed cells; lanes 4 and 8, the Pj fragment; lane 9, rabbit skeletal muscle α-actin; lane 10, LPA_5T fragment; lane 11, SPA_5T fragment; lane 12, LPA_4T fragment; lane 13, LPA_3T fragment; lane 14, LP fragment; lane 15, A_5T fragment; lane 16, P fragment; lane 17, P_N fragment; lane 18, P_CA_3 fragment. The percentages of polyacrylamide in the gels are provided below each panel, and the molecular weight standards are on the left. The highest molecular mass bands in lanes 1, 2 and 4, which were considered to be the full-length recombinant proteins, are indicated by open arrowheads, while the putative proteolytic products are indicated by closed arrowheads.

band with a molecular mass of 190 kDa (*21*), we considered the phenomenon that the migration rates of MAP4 and its fragments are slower than those expected from the primary structures to be an inherent property of the proteins. The skeletal muscle α-actin (Fig. 1B, lane 9) was electrophoretically pure.

Interaction between MAP4 and actin filaments

We first demonstrated the binding of the full-length MAP4 recombinant proteins to actin filaments by a differential-sedimentation assay (Fig. 2A). MAP4 protein/actin mixtures were incubated in MEM buffer, centrifuged at low speed to sediment the actin bundles and then centrifuged at high speed to sediment the actin filaments. None of the recombinant proteins precipitated by themselves (data not shown) and the actin filaments alone did not appear in the low-speed pellet (Fig. 2B, lane 1). Although neither of the full-length MAP4 isoforms appeared in the actin bundle fractions (Fig. 2A, lanes 1 and 4), they co-precipitated with the actin filaments (Fig. 2A, lanes 2 and 5) along with their degraded products (lower molecular mass bands, indicated by closed arrowheads), clearly indicating the interaction between MAP4 and actin. Some of the

Downloaded from http://jb.oxfordjournals.org/ at Changhua Christian Hospital on September 26, 2012

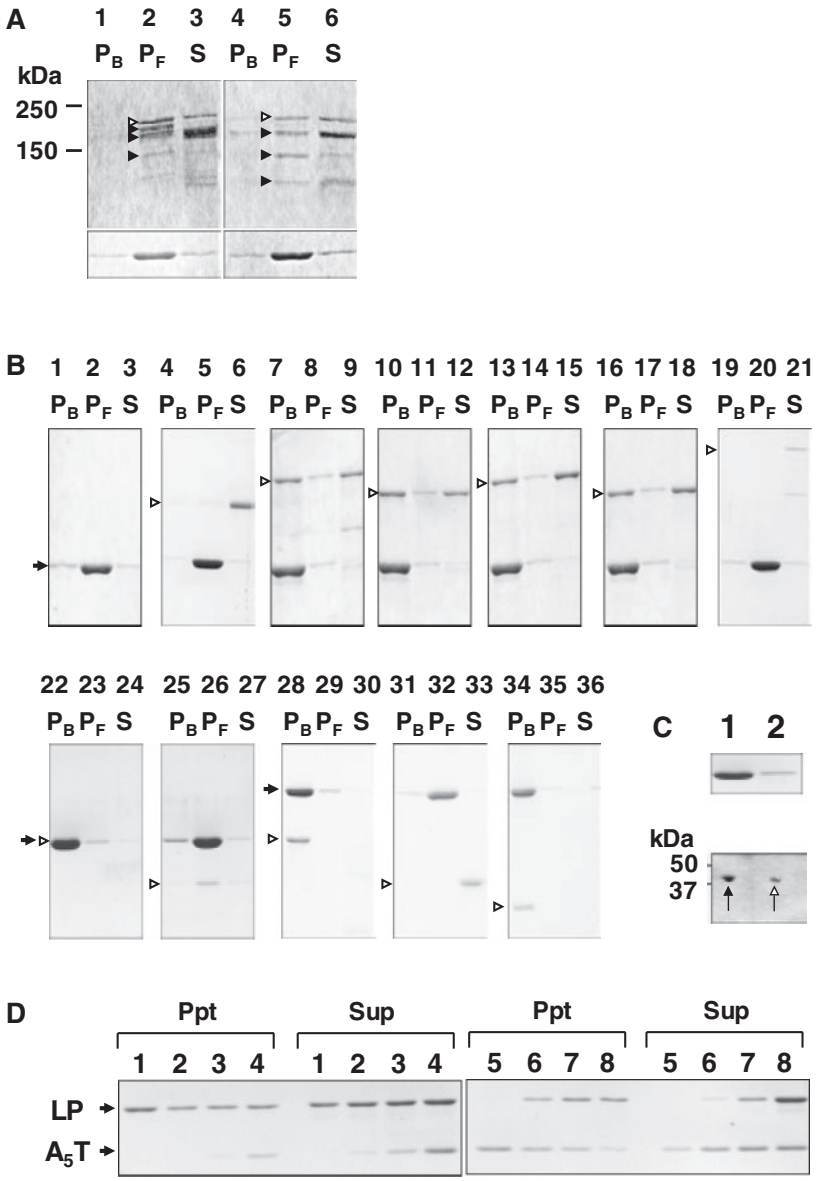

Fig. 2 SDS-PAGE analysis of the binding of full-length MAP4 and its truncated proteins to actin filaments. In A–D, the gels were stained with CBB. (A) The supernatants and the pellets of the centrifuged (full-length MAP4)/actin mixtures were analysed on 7.5% (for full-length MAP4, upper panels) and 14% (for actin, lower panels) polyacrylamide gels. Lanes 1–3, 4 μM actin and 2 μM MAP4-LP; lanes 4–6, 4 μM actin and 2 μM MAP4-SP. P_B, the low-speed pellet (actin bundle fraction); P_F, the high-speed pellet (actin filament fraction); S, the supernatant (monomeric actin fraction). The actin-bound MAP4 isoforms and their degraded polypeptides are indicated by the open and closed arrowheads, respectively. (B) Sedimentation assay of actin incubated in the absence (lanes 1–3) or presence of 2 μM BSA (lanes 4–6), LPA_5T fragment (lanes 7–9), SPA_5T fragment (lanes 10–12), LPA_4T fragment (lanes 13–15), LPA_3T fragment (lanes 16–18), Pj fragment (lanes 19–21), LP fragment (lanes 22–24), A_5T fragment (lanes 25–27), P fragment (lanes 28–30), P_N fragment (lanes 31–33), or P_CA_3 fragment (lanes 34–36). P_B, P_F and S represent the same fractions as in A. Aliquots of the resultant P_B, P_F and S fractions were electrophoresed on 10% (lanes 1–21), 12.5% (lanes 22–27) or 14% (lanes 28–36) polyacrylamide gels. Open arrowheads mark the positions of the bands corresponding to MAP4 fragments or BSA and arrows represent the electrophoretic position of actin. The mobility of the LP fragment is nearly identical to that of actin under these conditions. (C) Identification of the LP fragment in the actin pellet in B lane 22. Upper panel, the actin pellet in B lane 22 was boiled and centrifuged. The resultant pellet (actin) (lane 1) and the supernatant (the LP fragment) (lane 2) were subjected to SDS–PAGE. Lower panel, the actin pellet in B lane 22 was analysed by two-dimensional gel electrophoresis. The actin and LP fragment spots are indicated by closed and open arrows, respectively. (D) Competition between the LP and A_5T fragments for actin filament binding. All samples contained 20 μM actin. The concentrations of the LP fragment (lanes 1–4) and the A_5T fragment (lanes 5–8) were 8 μM. The concentrations of the added A_5T or LP fragment were lanes 1 and 5, 0 μM; lanes 2 and 6, 2 μM; lanes 3 and 7, 4 μM; lanes 4 and 8, 8 μM. Precipitates were boiled and centrifuged to reveal the band of the LP fragment bound to actin filaments. The resultant supernatants, labelled as Ppt, were fractionated on gels. LP and A_5T represent the electrophoretic positions of the LP and A_5T fragment, respectively.

degraded bands preferentially appeared in the supernatant (Fig. 2A, lanes 3 and 6), suggesting that they lost the actin-binding domain(s) through degradations.

Since MAP2 and tau reportedly bind to actin filaments through their microtubule-binding domains (*11–14*), we next tested whether this is also the case for MAP4, using truncated fragments (Fig. 2B, lanes 1–21). BSA, used as a negative control, did not co-precipitate with the actin filaments (Fig. 2B, lane 5). As expected, the microtubule-binding domain

Downloaded from http://jb.oxfordjournals.org/ at Changhua Christian Hospital on September 26, 2012

fragments (LPA_5T, SPA_5T, LPA_4T and LPA_3T) sedimented with the actin filaments (Fig. 2B, lanes 7, 10, 13, and 16), whereas the Pj fragment, consisting of the projection domain, did not (Fig. 2B, lane 20). However, the recovery patterns of the MAP4 fragments in the pellet were quite different from those of the full-length proteins: when the MAP4 fragments were mixed with the actin filaments and centrifuged at low speed, almost all of the actin and the fragments were recovered in P_B (Fig. 2B, lanes 7, 10, 13 and 16).

To identify the subdomain(s) responsible for actin binding, we then tested the activity of the first half subdomain (the entire Pro-rich region) fragment (LP) and the second half subdomain (the Repeat and Tail regions) fragment (A_5T) of the microtubule-binding domain. Although the LP fragment and actin were absent from the supernatant (Fig. 2B, lane 24), the two proteins could not be identified clearly in the pellet (Fig. 2B, lane 22), because of their similar electrophoretic mobility. Therefore, we fractionated the pellet (Fig. 2B, lane 22) based on the heat stability or the surface charge of the proteins (Fig. 2C). When the pellet was boiled and centrifuged, the heat-labile actin was recovered in the pellet, while the heat-stable LP fragment was present in the supernatant (Fig. 2C, upper panel). Two-dimensional gel electrophoresis also revealed the two proteins in the pellet (Fig. 2C, lower panel). Consequently, we concluded that the LP fragment binds to the actin filaments and forms bundles. Meanwhile, the A_5T fragment and actin were recovered in the high-speed pellet (Fig. 2B, lane 26). Since both the Pro-rich and downstream regions (the Repeat and Tail regions) possess actin-binding activity, the activities of the two regions were compared (Fig. 2D). The competition between a fixed amount of the LP fragment and various concentrations of the A_5T fragment demonstrated that a large amount of the LP fragment could be recovered in the pellet fraction, even in the presence of an equal amount of the A_5T fragment (Fig. 2D, left panel). About one-third of the LP fragment remained bound in the presence of the A_5T fragment. On the other hand, the A_5T fragment was almost completely released from the actin filaments by the addition of an equal amount of the LP fragment (Fig. 2D, right panel).

Finally, additional MAP4 fragments, the P, P_N, P_CA_3 fragments, were examined to refine the location of the active site in the Pro-rich region (Fig. 2B, lanes 28–36). Almost all of the P fragment was recovered in the pellet (Fig. 2B, lane 28), suggesting that residues 579–646 and 867–880 are dispensable. The P_N fragment hardly bound to the actin filaments (Fig. 2B, lane 33), consistent with the result that the SPA_5T fragment, which lacks this portion, displays the actin-binding activity (Fig. 2B, lane 10). The PcA_3 fragment associated well with the actin filaments (Fig. 2B, lane 34). Consequently, the actin-binding activity of MAP4 resides within residues 803–866 of the Pro-rich region.

Aliquots of the MAP4 protein/actin mixtures were negatively stained and examined by electron microscopy (Fig. 3). The actin filaments alone were curved and partially entangled, while they appeared to be rigid and straight in the presence of MAP4 (Fig. 3A). We could not detect any signs of actin-bound MAP4 molecules since the diameter of the actin filaments seemed uniform at this resolution. Unlike other MAPs such as MAP2 and tau, which reportedly induce thick actin bundles (*11–14*, *24*), actin bundles were rarely observed, consistent with the absence of low-speed pellets (Fig. 2A, lanes 1 and 4). The microtubule-binding domain fragments (LPA_5T, SPA_5T, LPA_4T and LPA_3T) and the subdomain fragments containing residues 803–866 (LP, P and PcA_3) induced thick actin-bundles with various diameters (~200 nm) (Fig. 3B). Although single filaments were sometimes observed, the majority of the filaments formed bundles. There was no detectable difference in the appearances of the actin bundles induced by these MAP4 fragments. As expected, actin bundles were not observed in the A_5T fragment sample, consistent with the absence of the fragment in the low-speed pellet (Fig. 2B, lane 25).

The dissociation constants (K_d) between each of the four microtubule-binding domain fragments (LPA_5T, SPA_5T, LPA_4T and LPA_3T) and actin were within the same order of magnitude (Table I), suggesting that a common actin-binding site is retained in these fragments. The fact that the affinities of the MAP4 fragments for actin filaments were similar to their affinities for microtubules, determined by the same method (*3*, *4*), indicated the physiological significance of the interaction. The binding stoichiometries of the MAP4 fragments (Table I) were most reasonably interpreted as 1 : 3 (MAP4/actin).

Since the activities of the four microtubule-binding domain fragments were quite similar (Fig. 2B, Fig. 3B and Table I), we considered these MAP4 isoforms to bind to the actin filaments by a common mechanism. We, therefore, used only one fragment (LPA_5T) in the following examinations. The intracellular concentration of MAP4 is much lower than that of actin (*21*, *25*), and thus the MAP4 fragment concentration was reduced to a 1:200 molar ratio of the fragment to actin (Fig. 4A). The bands of the fragments were still detected in the pellets (Fig. 4A, lane 5). When the MEM buffer was replaced by another buffer with physiological ionic strength (PBS), ~50% of the LPA_5T fragment co-precipitated with the actin filaments (Fig. 4A, lane 7). We also tested the actin-binding activity of MAP4 in the presence of tubulin (Fig. 4B). The tubulin and MAP4 fragment concentrations were kept below the critical concentration for microtubule assembly, as revealed by the absence of microtubules in the pellet (Fig. 4B, lane 1). The addition of actin resulted in the recovery of about half of the tubulin in the pellet (Fig. 4B, lane 3). When the concentration of the LPA_5T fragment was increased, almost all of the tubulin was recovered in the pellet (Fig. 4B, lane 5). The precipitable tubulin probably bound to the actin filaments through the LPA_5T fragment. The sample corresponding to Fig. 4B, lane 5, was observed by electron microscopy with immunogold-labelled MAP4 (Fig. 4C). Gold grains were often seen along the actin filaments, and the blurred staining surrounding the grains may be interacting tubulin. No microtubules were found.

Downloaded from http://jb.oxfordjournals.org/ at Changhua Christian Hospital on September 26, 2012

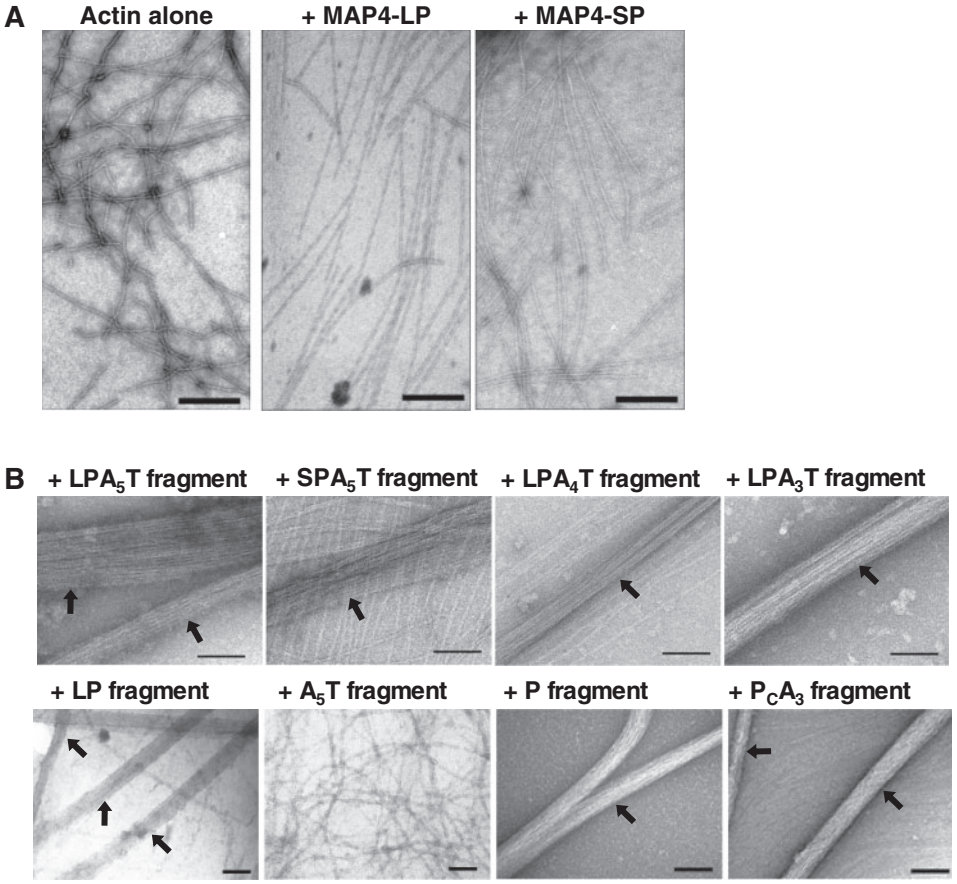

Fig. 3 Electron micrographs of negatively stained preparations of actin filaments, in the presence of full-length MAP4 or its truncated fragments. Actin (4 μM) was polymerized in the presence of 2 μM of the full-length MAP4 (A), or the truncated fragments (B), and was observed by electron microscopy. Arrows represent actin bundles. Bars are 100 nm.

Table I. K_d values and stoichiometries of the binding between MAP4 fragments and actin.

Fragment name	LPA_5T	SPA_5T	LPA_4T	LPA_3T
K_d (μM)	0.08	0.14	0.10	0.09
Stoichiometry	0.31	0.35	0.30	0.29

In addition, there were far fewer actin bundles present, as compared to Fig. 3. Although this is primarily due to our choice of a frame in which the gold grains could be easily observed, the population of the bundles actually seemed to be lower than that of the tubulin-free sample. The actin-bundling activity of the fragment may be reduced in the presence of tubulin. In any case, we can fairly conclude from Figs. 4B and 4C that MAP4 binds to both actin filaments and tubulin simultaneously. These results suggested that MAP4-actin binding is physiologically possible within cells.

Detection of the actin-binding activity of MAP4 by chemical crosslinking

When the LPA_5T fragment was treated with 5 mM of EDC, a 'zero-length cross-linker', no major band reactive to the anti-MAP4 antiserum appeared, except for the 73 kDa, original LPA_5T fragment band (Fig. 5, lane 6). In the case of actin (Fig. 5, lane 1), a 42-kDa band and a faint 125-kDa band were detected. When the mixture of actin and MAP4 fragment was subjected to the cross-linking, new bands appeared with apparent molecular masses >250 kDa, which reacted with the anti-MAP4 antiserum (Fig. 5, lanes 3 and 7). In the presence of cytochalasin D, the amounts of high-molecular-mass bands observed in Fig. 5, lane 3, were markedly reduced (Fig. 5, lane 4), while the 125-kDa band was intensified and a new 85-kDa band appeared. These two bands were reactive with the anti-actin antibody (Fig. 5, lane 9), but not the anti-MAP4 antiserum (Fig. 5, lane 8), suggesting that they were actin trimers and dimers, respectively. The MAP4 fragment is likely to bind preferably to filamentous actin rather than to monomeric or oligomeric actin. Consistent with this view, the MAP4 fragment was not adsorbed to DNase-I conjugated resin (data not shown).

The effect of MAP4-binding on the properties of actin filaments

The morphologies of the MAP4-bound actin were further analysed using lower concentrations of MAP4 fragments (Fig. 6). In the absence of the fragment, many of the actin filaments were wavy and tangled (Fig. 6A). Straight filaments were sometimes found

Downloaded from http://jb.oxfordjournals.org/ at Changhua Christian Hospital on September 26, 2012

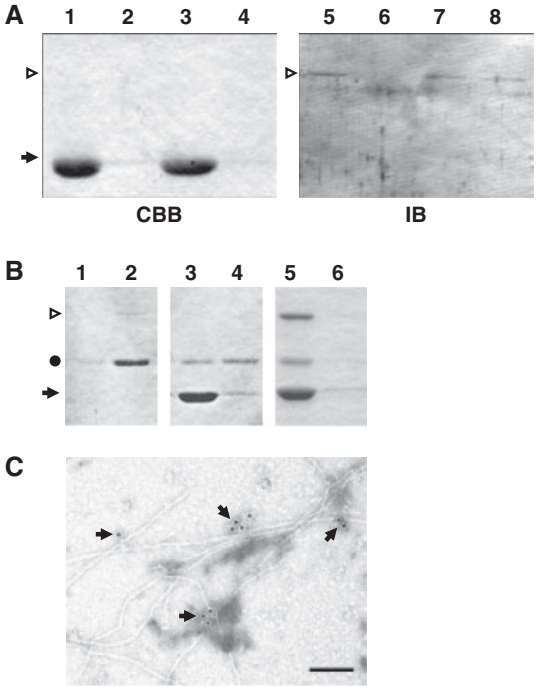

Fig. 4 Effect of the molar ratio of MAP4 fragment to actin and the presence of tubulin on the actin-binding activity of MAP4 fragment. In A and B, the open arrowhead marks the position of the LPA_5T fragment, and the arrow represents the position of actin. (A) Sedimentation assay at a low concentration of the LPA_5T fragment: lanes 1 and 2, the mixtures of the LPA_5T fragment (0.1 μM) and actin filaments (20 μM) in MEM or lanes 3 and 4, PBS; lanes 1 and 3, pellets; lanes 2 and 4, supernatants; lanes 5–8, the same aliquots of lanes 1–4 were electrophoresed and immunoblotted with anti-MAP4 antiserum. (B) Binding of the LPA_5T fragment to actin in the presence of 2 μM tubulin. The concentrations of actin are lanes 1 and 2, 0 μM; lanes 3–6, 10 μM. The concentrations of the LPA_5T fragment are lanes 1–4, 0.1 μM; lanes 5 and 6, 2 μM. The mixtures were ultra-centrifuged, and the resultant precipitates (odd-numbered lanes) and supernatants (even-numbered lanes), were electrophoresed. The dot represents the electrophoretic position of tubulin. (C) An electron micrograph of a negatively stained preparation corresponding to Fig. 4B, lane 5. The sample was immunolabelled by rabbit anti-MAP4 antiserum followed by 10-nm gold-coupled goat anti-rabbit IgG, and was observed by electron microscopy. Arrows represent gold grains. Bars are 100 nm.

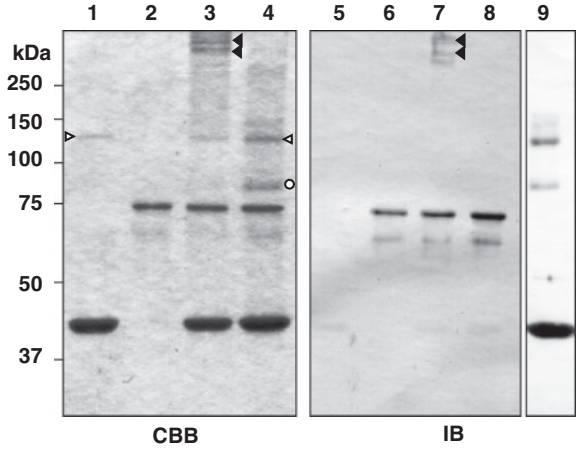

Fig. 5 EDC-cross-linking of actin to the LPA_5T fragment. The cross-linked products were electrophoresed and stained with CBB (lanes 1–4) or immunoblotted using anti-MAP4 antiserum (lanes 5–8) or an anti-actin antibody (lane 9). Lanes 1 and 5, actin alone; lanes 2 and 6, LPA_5T fragment alone; lanes 3 and 7, actin and LPA_5T fragment; lanes 4, 8 and 9, actin, LPA_5T and cytochalasin D. Closed arrowheads indicate the putative actin-MAP4 complex. Open arrowheads and the circle mark the putative actin oligomers.

aligned side by side (open arrows), but they did not form bundles. Some filaments were broken into short pieces, as revealed by the abundance of filament tips observed in a single panel (Fig 6A, closed arrowheads). The appearance of the actin filaments in the presence of 0.01 μM of the LPA_5T fragment was similar to that of the control sample (data not shown). The actin filament morphology started to change when 0.1 μM of the LPA_5T fragment was present (molar ratio of the fragment to actin was 1 : 40). Although thick bundles were still absent, fewer filaments were tangled or broken. The number of actin tips was also reduced in the presence of the MAP4 fragment (Fig. 6B). More than 50 actin filaments were randomly chosen from electron micrographs, and their lengths were measured (data not shown): ~80% of the actin filaments in the presence of the fragment were longer than 1 μm, whereas >60% of the control actin filaments were shorter than 1 μm. Many thick actin bundles (~20–100 nm in diameter) were detected when the concentration of the fragment was increased to 0.5 μM, and the unbundled filaments became much straighter (Fig. 6A). Tangled filaments were not found. We quantified these phenomena, by employing a set frame of 25 nm × 300 nm as a criterion (Fig. 6C). The percentage of straight filaments in the 0.5 μM LPA_5T sample (72%) was larger than those of the control (26%) and the sample with 0.1 μM of LPA_5T (30%) (Fig. 6D).

The putative actin-binding site(s) on MAP4

He *et al.*(*14*) reported the binding of the Pro-rich region fragment of human tau to actin, and the basis of the interaction was the electrostatic force between the positively charged residues of tau and the negatively charged residues of actin. In order to search for positively charged clusters in the MAP4 Pro-rich region, we compared the sequences of the bovine, human and murine MAP4 Pro-rich regions (Fig. 7). Although the Pro-rich regions are interspecifically less conserved than the Repeat regions (>88% similarity (*2*)), the positions of the basic residues, which are considered to be involved in actin binding, are completely conserved (Fig. 7). A sequence comparison between MAP4 and the tau Pro-rich regions revealed two weakly conserved, short sequences containing positively charged residues, [(S/T)R(A/V/S)(R/K) and KK(P/V)(T/A)(A/V/S)(A/T/V)(K/R)], despite the lack of overall sequence homology among the Pro-rich regions of MAP4 and tau. The basic local alignment search tool (BLAST) analysis of the MAP4 Pro-rich region revealed no similarity with known actin-binding proteins, and no structural motifs or folds were detected in this region (data not shown).

Downloaded from http://jb.oxfordjournals.org/ at Changhua Christian Hospital on September 26, 2012

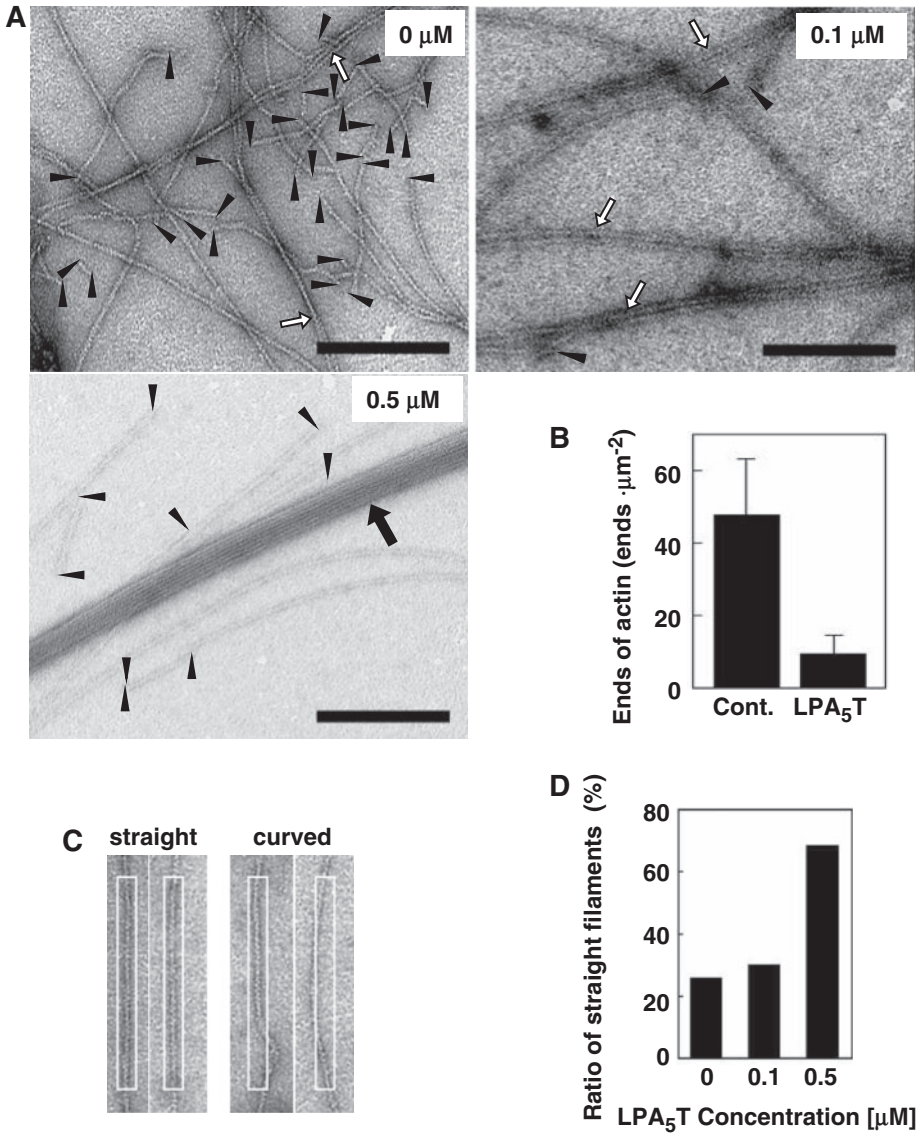

Fig. 6 Effect of the MAP4 fragment (LPA_5T) on the morphology of actin filaments. (A) Actin (4 μM) was polymerized in the presence of various concentrations (0, 0.1 and 0.5 μM) of the LPA_5T fragment and was observed by electron microscopy. Arrowheads indicate the tips of actin filaments. Open arrows mark filaments attached to neighbouring filaments. The closed arrow represents an actin bundle. Bars are 200 nm. (B) The number of actin ends was counted from the microphotographs. *Ordinate* is the average number of actin ends per 1 μm^2. Cont. and LPA_5T are the data of the control (actin alone) sample and 0.1 μM of the LPA_5T fragment-containing sample, respectively. Error bars indicate standard deviations. (C) Typical micrographs of actin filaments judged as straight or curved. More than 100 randomly chosen actin filaments were fitted into a set frame (*boxes*) corresponding to an area of 25×300 nm. (D) The ratio of actin filaments that fit in the frame.

Discussion

In this study, we have demonstrated that MAP4 interacts with actin filaments *in vitro*. Our sedimentation assays, chemical cross-linking and electron microscopic observations revealed that two full-length MAP4 isoforms, as well as truncated fragments containing the microtubule-binding domain, bind to actin filaments. The critical region for the actin binding was situated within the C-terminal part (residues 803–866) of the Pro-rich region. The apparent K_d and the stoichiometry were about 0.1 μM and 1 : 3 (MAP4/actin), respectively. The MAP4-actin interaction is highly probable in living cells since it occurs at a relatively low concentration of MAP4, and even in the presence of tubulin. The MAP4-bound actin filaments became straight and bundled, which may be physiologically important. A multiple sequence alignment of the MAP4/tau Pro-rich regions revealed clusters of positively charged residues, which may be responsible for actin binding.

The actin-binding site of MAP4 lies in the microtubule-binding domain, similar to the other MAPs (MAP2 and tau) (*11–14*, *24*). Unlike MAP2 and tau, however, the full-length MAP4 did not induce actin bundles. Since the LP, P and P_CA_3 fragments bound to actin filaments with high efficiency, the portion(s) responsible for actin binding is localized in the overlapping part of the three fragments (residues 803–866). Although the weak binding of the A_5T fragment suggests that another actin-binding site(s) may

Downloaded from http://jb.oxfordjournals.org/ at Changhua Christian Hospital on September 26, 2012

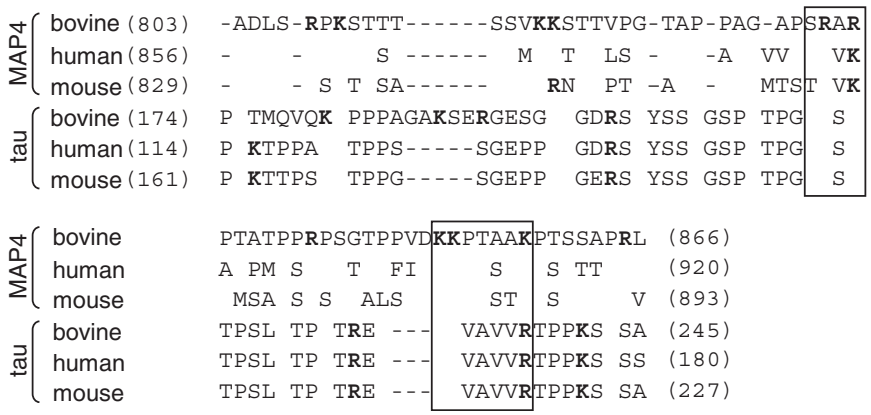

Fig. 7 Comparison of the Pro-rich region sequences between MAP4 and tau. The C terminal partial sequences of the Pro-rich regions for bovine, human and murine MAP4 and tau were aligned. The ovine MAP4 sequence was used as the standard for comparison, and only the differences between the bovine MAP4 sequence and the other MAP4/tau sequences are indicated. Basic residues are indicated by *bold* type. Arabic numerals are the amino acid residue numbers of the proteins. Sequence gaps are indicated by *dashes*. The short consensus sequences, (S/T)R(A/V/S)(R/K) and KK(P/V)(T/A)(A/S/V)(A/T/V)(K/R), are surrounded by open squares.

reside in the Repeat and/or Tail region, the activity of the Repeat and/or Tail region is considered to contribute minimally to the overall activity of the intact MAP4, for the following reasons: the affinity of the A_5T fragment was considerably lower than that of the Pro-rich region (Fig. 2D), the A_5T fragment did not induce actin bundles (Fig. 3B), and various deletions in the Repeat region exerted a marginal effect on the binding affinity (Table I). Consequently, the major actin-binding site(s) are considered to be present within the C-terminal part of the Pro-rich region. Nevertheless, the electrostatic natures of the Pro-rich region and the Repeat region are very much similar: the theoretical pI values of the N-terminal (residues 641–717) and C-terminal (residues 803–866) parts of the Pro-rich region and the Repeat region (residues 881–1013) of bovine MAP4 were 10.2, 11.9 and 10.9, respectively, indicating that the basis of the MAP4–actin interaction cannot simply be explained by the electrostatic force. Some site-specific associations may be necessary for the binding, and the two weakly conserved short sequences revealed by the sequence comparison (Fig. 7) are plausible candidates.

In the presence of MAP4 or its truncated fragments, changes in both the shape and length of the actin filaments were observed. These morphological events can be explained by the modulation of the mechanical strength of actin filaments. A similar effect reportedly occurs upon tropomyosin binding: tropomyosin binds on the side of actin filaments, inhibits the spontaneous severing of actin filaments *in vitro* and stabilizes the cytoplasmic architectures formed by actin filaments (*26*). We also observed actin bundling in the presence of some of the truncated fragments, but it should be noted that the actin filaments in the presence of full-length MAP4 did not form bundles (Fig. 2A and 3 A). Bovine tau and MAP2c, which both have a projection domain shorter than 200 residues, induced actin bundling, while bovine MAP2, with a long projection domain (~1,500 residues long), did not (*24*, *13*). A certain length of the projection domain may serve as a steric hindrance against bundling, suggesting that the actin-bundling activity is not an innate property of full-length MAP4. We previously reported that MAP4 binding to microtubules alters their surface properties to form microtubule bundles (*3*). The MAP4 fragments may exert a similar effect on the surface properties of actin filaments. Consequently, MAP4 affects the mechanical strength and the surface properties of actin filaments, which may influence the interactions between actin filaments, actin filaments and microtubules, or actin filaments and other actin-binding factors.

To date, the expression of several MAP4 isoforms, generated by alternative splicing, has been reported in various cells and tissues (*2–4*). Among these isoforms, MAP4-SP is characteristically concentrated in developing neurites (*6*). As described in the *Introduction*, MAP4-SP may interact with actin filaments there, and the deletion in MAP4-SP may enhance the actin-binding activity of MAP4. Our *in vitro* assays demonstrated that MAP4-SP binds to actin filaments. However, MAP4-LP also showed actin-binding activity, indicating that the activity is an intrinsic property of MAP4, and is not specific to one particular isoform. Consequently, the distribution of MAP4-SP within an actin-rich region in neurites cannot be ascribed to its affinity to actin filaments, but may depend on other cellular factors in neurites. Nevertheless, the finding of the MAP4–actin interaction is still important for the physiological function of MAP4-SP. Since the presence of MAP4 into the actin-rich cytoplasmic area has been most remarkably observed in the case of MAP4-SP in neurites (*6*), the contribution of MAP4-SP to the dynamics and/or the rearrangement of the neuronal actin cytoskeleton have become even more probable. Further studies on the cytoplasmic dynamics of MAP4-SP and actin in cultured neural cells are now in progress.

Acknowledgements

Authors thank Dr Brenda Yoshinaga (SKYBAY Scientific Editing) for reading the manuscript.

Downloaded from http://jb.oxfordjournals.org/ at Changhua Christian Hospital on September 26, 2012

Conflict of interest
None declared.

References

1. Tokuraku, K., Katsuki, M., and Kotani, S. (2002) Structural and functional analyses of microtubule-associated protein 4. *Recent Res. Dev. Biochem.* **3**, 315–333
2. West, R.R., Tenbarge, K.M., and Olmsted, J.B. (1991) A model for microtubule-associated protein 4 structure. Domains defined by comparisons of human, mouse, and bovine sequences. *J. Biol. Chem.* **266**, 21886–21896
3. Tokuraku, K., Matsushima, K., Matui, T., Nakagawa, H., Katsuki, M., Majima, R., and Kotani, S. (2003) The number of repeat sequences in microtubule-associated protein 4 affects the microtubule surface properties. *J. Biol. Chem.* **278**, 29609–29618
4. Matsushima, K., Aosaki, M., Tokuraku, K., Hasan, M.R., Nakagawa, H., and Kotani, S. (2005) Identification of a neural cell specific variant of microtubule-associated protein 4. *Cell Struct. Funct.* **29**, 111–124
5. Hasan, M.R., Jin, M., Matsushima, K., Miyamoto, S., Kotani, S., and Nakagawa, H. (2006) Differences in the regulation of microtubule stability by the pro-rich region variants of microtubule-associated protein 4. *FEBS Lett.* **580**, 3505–3510
6. Hasan, M.R., Matsushima, K., Jin, M., Nakagawa, H., Miyamoto, S., and Kotani, S. (2006) Functional analyses of a neural cell specific variant of microtubule-associated protein 4. *Sci. J. Kanagawa Univ.* **17**, 3–11
7. Tokuraku, K., Okuyama, S., Matsushima, K., Ikezu, T., and Kotani, S. (2010) Distinct neuronal localization of microtubule-associated protein 4 in the mammalian brain. *Neurosci. Lett.* **484**, 143–147
8. Goode, B.L., Drubin, D.G., and Barnes, G. (2000) Functional cooperation between the microtubule and actin cytoskeletons. *Curr. Opin. Cell Biol.* **12**, 63–71
9. Dent, E.W. and Gertler, F.B. (2003) Cytoskeletal dynamics and transport in growth cone motility and axon guidance. *Neuron* **40**, 209–227
10. Halpain, S. and Dehmelt, L. (2006) The MAP1 family of microtubule-associated proteins. *Genome Biol.* **7**, 224
11. Griffith, L.M. and Pollard, T.D. (1982) The interaction of actin filaments with microtubules and microtubule-associated proteins. *J. Biol. Chem.* **257**, 9143–9151
12. Moraga, D.M., Nuñez, P., Garrido, J., and Maccioni, R.B. (1993) A tau fragment containing a repetitive sequence induces bundling of actin filaments. *J. Neurochem.* **61**, 979–986
13. Roger, B., Al-Bassam, J., Dehmelt, L., Milligan, R.A., and Halpain, S. (2004) MAP2c, but not tau, binds and bundles F-actin via its microtubule binding domain. *Curr. Biol.* **14**, 363–371
14. He, H.J., Wang, X.S., Pan, R., Wang, D.L., Liu, M.N., and He, R.Q. (2009) The proline-rich domain of tau plays a role in interactions with actin. *BMC Cell Biol.* **10**, 81
15. Murofushi, H., Kotani, S., Aizawa, H., Hisanaga, S., Hirokawa, N., and Sakai, H. (1986) Purification and characterization of a 190-kD microtubule-associated protein from bovine adrenal cortex. *J. Cell. Biol.* **103**, 1911–1919
16. Yoshida, T., Imanaka-Yoshida, K., Murofushi, H., Tanaka, J., Ito, H., and Inagaki, M. (1996) Microinjection of intact MAP-4 and fragments induces changes of the cytoskeleton in PtK2 cells. *Cell Motil. Cytoskeleton* **33**, 252–262
17. Lázaro-Diéguez, F., Aguado, C., Mato, E., Sánchez-Ruíz, Y., Esteban, I., Alberch, J., Knecht, E., and Egea, G. (2008) Dynamics of an F-actin aggresome generated by the actin-stabilizing toxin jasplakinolide. *J. Cell Sci.* **121**, 1415–1425
18. Spudich, J.A. and Watt, S. (1971) The regulation of rabbit skeletal muscle contraction. I. Biochemical studies of the interaction of the tropomyosin–troponin complex with actin and the proteolytic fragments of myosin. *J. Biol. Chem.* **246**, 4866–4871
19. Lowry, O.H., Rosebrough, N.J., Farr, A.L., and Randall, R.J. (1951) Protein measurement with the folin phenol reagent. *J. Biol. Chem.* **193**, 265–275
20. Laemmli, U.K. (1970) Cleavage of structural proteins during the assembly of the head of bacteriophage T4. *Nature* **277**, 680–685
21. Kotani, S., Murofushi, H., Maekawa, S., Sato, C., and Sakai, H. (1986) Characterization of microtubule-associated proteins isolated from bovine adrenal gland. *Eur. J. Biochem.* **156**, 23–29
22. Meyer, R.K. and Aebi, U. (1990) Bundling of actin filaments by alpha-actinin depends on its molecular length. *J. Cell Biol.* **110**, 2013–2024
23. Tokuraku, K., Katsuki, M., Nakagawa, H., and Kotani, S. (1999) A new model for microtubule-associated protein (MAP)-induced microtubule assembly. The Pro-rich region of MAP4 promotes nucleation of microtubule assembly in vitro. *Eur. J. Biochem.* **259**, 158–166
24. Kotani, S., Nishida, E., Kumagai, H., and Sakai, H. (1985) Calmodulin inhibits interaction of actin with MAP2 and Tau, two major microtubule-associated proteins. *J. Biol. Chem.* **260**, 10779–10783
25. Bulinski, J.C. and Borisy, G.G. (1980) Microtubule-associated proteins from cultured HeLa cells. Analysis of molecular properties and effects on microtubule polymerization. *J. Biol. Chem.* **255**, 11570–11576
26. Ish ikawa, R. and Kohama, K. (2007) Actin-binding proteins in nerve cell growth cones. *J. Pharmacol. Sci.* **105**, 6–11

Downloaded from http://jb.oxfordjournals.org/ at Changhua Christian Hospital on September 26, 2012